Microfluid Nanofluid (2011) 10:1069–1078
DOI 10.1007/s10404-010-0735-8

ORIGINAL PAPER

An efficient microfluidic sorter: implementation of double meandering micro striplines for magnetic particles switching

Tian Fook Kong · Huan Shin E · Hendrik Santoso Sugiarto · Hwi Fen Liew · Xinghua Wang · Wen Siang Lew · Nam-Trung Nguyen · Yong Chen

Received: 30 August 2010 / Accepted: 8 November 2010 / Published online: 28 November 2010

Abstract The ability to trap, manipulate, and separate magnetic beads has become one of the key requirements in realizing an integrated magnetic lab-on-chip biosensing system. In this article, we present the design and fabrication of an integrated magneto-fluidic device for sorting magnetic particles with a sorting efficiency of up to 95%. The actuation and manipulation of magnetic beads are realized using microfabricated square meandering current-carrying micro striplines. The current is alternated between two neighboring micro striplines to switch the magnetic beads to either one of the two outlets. We performed a series of parametric study to investigate the effect of applied current, flow rate, and switching frequency on the sorting efficiency. Experimental results reveal that the sorting efficiency is proportional to the square of current applied to the stripline, and decreases with increasing buffer flow rate and switching frequency. Such phenomena agree well with our theoretical analysis and simulation result. The fastest switching rate, which is limited by the microchannel geometry and bead velocity, is 2 Hz.

T. F. Kong · H. S. E · H. S. Sugiarto · H. F. Liew · X. Wang · W. S. Lew (✉)
School of Physical and Mathematical Sciences, Nanyang Technological University, 21 Nanyang Link, Singapore 637371, Singapore
e-mail: wensiang@ntu.edu.sg

N.-T. Nguyen
School of Mechanical and Aerospace Engineering, Nanyang Technological University, 50 Nanyang Avenue, Singapore 639798, Singapore

Y. Chen
Ecole Normale Supérieure, CNRS-ENS-UPMC UMR 8640, 24 rue Lhomond, 75005 Paris, France

Keywords Magnetofluidic · Magnetic bead · Sorting · Switching · Micro stripline

1 Introduction

In recent years, the development of microfluidic technology aims at application in lab-on-a-chip (LOC) or micro total analysis systems (μTAS). The novel introduction of magnetism in microfluidic has enabled a myriad of new opportunities in terms of technological innovation in LOC (Pamme 2005), especially in biological micro-electro-mechanical systems (BioMEMS) (Bashir 2004). The key advantage of using magnetism in biosensors is the non-contact nature of the magnetic forces with biological samples (Pamme 2005). Magnetic particles (such as superparamagnetic beads) and ferrofluids (Nguyen et al. 2006) can be manipulated remotely with magnetic forces induced either by a permanent magnet or an electromagnet placed in close proximity. However, one of the most challenging tasks for magnetic actuation in microfluidic systems is to obtain well-defined magnetic forces on magnetic particles (Ramadan et al. 2006).

Thus far, many biological related applications for an integrated magnetic LOC system have been reported. These applications includes: targeted cancer-cell destruction (Kim et al. 2010), virus detection (Lee et al. 2008), biochemical detection for protein analysis (Choi et al. 2002), immuoassays (Bange et al. 2005; Lim and Zhang 2007), cell seperation (Inglis et al. 2004), magnetic labels, and deoxyribonucleic acid (DNA) purification (Gijs 2004). Magnetic beads have become one of the indispensible components in these integrated magnetic devices. The beads are commercially available and can be functionalized by tagging with desired bio-molecules such as DNA,

antibody, and protein (Pamme 2005; Gijs et al. 2010). Recently, extensive works have been carried out in understanding the trapping (Lee et al. 2001, 2004; Liu et al. 2007b), transport (Rida et al. 2003; Speetjens and de Boeck 2004), manipulation (Smistrup et al. 2006; Shikida et al. 2009; Wang et al. 2006), and separation (Choi et al. 2001; Deng et al. 2002) behaviors of magnetic beads.

The magnetic force acting on a magnetic bead is proportional to the bead volume and the magnetic field gradient (Pamme 2005; Gijs 2004). Pamme and Wilhelm (2006) has demonstrated an on-chip free-flow magnetic beads separation based on magnetophoresis sorting. Magnetic beads of various sizes experience different strengths of magnetic forces due to its bead diameter and magnetic susceptibility. Thus, the magnetic beads are deflected and separated into different outlets. As the diameter of a magnetic bead ranges from several hundreds of nanometer to several micrometers, the magnetic field generated by electromagnet is generally weak (0–10 mT) (Shevkoplyas et al. 2007). The magnetic force exerted on a magnetic bead is in the order of 10^{-12} N (Pamme 2005; Lee et al. 2007; Kose et al. 2009; Liu et al. 2007a). Ramadan et al. (2006) optimized the magnetic forces by enhancing the magnetic field gradient with the introduction of magnetic cores. Although the inclusion of the ferromagnetic cores would increase the force exerted onto the magnetic beads, the ferromagnetic layer has remanence once it is magnetized. The remanence effect is not desirable since beads will be trapped at these locations even when no current is applied to the striplines. Rong et al. (2006) reported an on-chip magnetic bead separator by incorporating pointed magnetic tips in the microsystem. Jiang et al. (2006) also worked on manipulating magnetic beads using current carrying micro striplines. Song et al. (2009) developed a microfluidic cell sorting system that incorporate joule heating and active cooling to maintain the microchannel at biocompatible temperature of 37°C.

In this study, we focused on developing an integrated magnetic bead switching device to switch the magnetic beads between two outlets. Such switching device is essential for separating two different bio-molecules tagged with superparamagnetic beads of different sizes or magnetic properties. By means of a giant magnetoresistance (GMR) sensor for detection, the magnetically labeled molecules could be distinguished and sorted to the desired outlets. Here, we present the design and fabrication of a bead separator that is relatively easy to fabricate, and, at the same time, achieve higher sorting efficiency. Our device is able to switch magnetic beads to the desired outlet solely by the magnetic forces generated by the on-chip micro stripline, without any magnetic core enhancement. The quantitative measurement of the effect of applied current, beads flow rate, and switching frequency has enabled us to understand the underlying physical mechanism of magnetic particle separation.

2 Materials and methods

2.1 Microchannel and magnetic stripline design

Current-carrying striplines have been used extensively for generating micromagnetic forces to actuate and manipulate magnetic particles. In this study, we demonstrate magnetic bead switching by using microfabricated square meandering micro stripline. Magnetic beads are switched either to the left or right by alternating the current supply to two neighbouring square meandering striplines in a microfluidic sorting chamber. The integrated magnetic bead separation device consists of two components: micro stripline electromagnet and polydimethylsiloxane (PDMS) microchannel. Figure 1a shows the overview of the microfluidic channel design, while Fig. 1b shows an optical microscope image of the microfluidic sorting chamber with square meandering micro stripline aligned and bonded beneath.

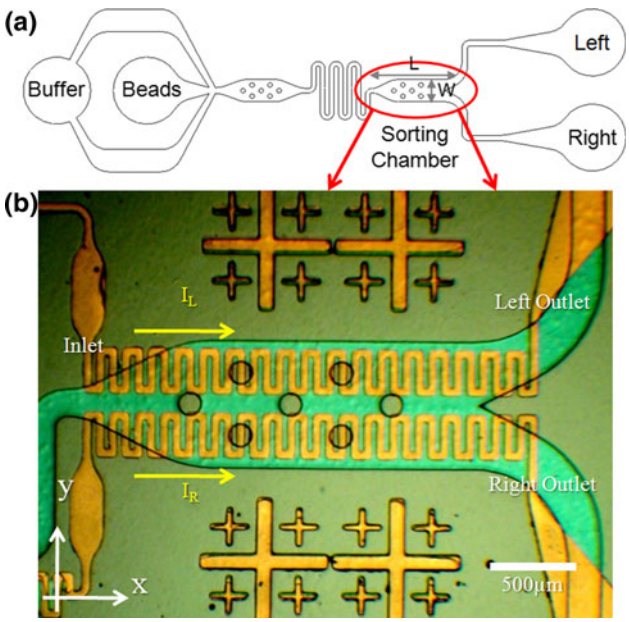

Fig. 1 **a** Microfluidic channel design. The magnetic beads are hydrodynamically focused in core stream, sandwiched by two buffer side streams. Without the presence of magnetic fields, the magnetic beads split and exit equally to the left and right outlets. The sorting chamber has a length, L of 3,500 μm and a width, W of 1,000 μm. **b** Optical micrograph of the sorting chamber with micro striplines aligned and bonded beneath. Magnetic forces are generated when the current I_L and I_R are applied to the left and right micro stripline, respectively. The y-component magnetic bead force plays an important role in determining the success rate of sorting the beads. The beads are forced to gradually change its flow path and choose a streamline closer to the field generating stripline

The widths of the striplines are 50 μm and have a height–width ratio of 3. There are in total 35 turns for the left and right striplines, respectively. The main sorting chamber measures 3,500 μm × 1,000 μm while the height of the microchannel is approximately 25 μm.

By means of hydrodynamic focusing, the magnetic beads are focused in core stream, and splits equally to the two outlets. When there are no magnetic forces acting on the beads, the beads flow with constant velocity and move according to the buffer's flow streamlines. With the presence of magnetic forces, the magnetic beads change their flow path and switch to another streamline closer to the field generating micro stripline. Thus, by gradually changing the flow path of the beads, we are able to direct the beads to a certain outlet. The success of switching the beads is determined by the strength of the magnetic force in the *y*-direction.

2.2 Device fabrication

The magnetic micro striplines were fabricated using standard photolithography process. First, a layer of approximately 20 μm thick AZ9260 (AZ Electronics, Japan) positive photoresist was patterned onto a silicon substrate with 300 nm thick silicon dioxide (SiO_2) layer. The photoresist was spun at 2,100 rpm with 80 s softbake at 110°C followed by a second spin of 1,600 rpm with 160 s softbake at the same baking temperature. The resist was then exposed with UV light (MJB4, SUSS MicroTec, Germany) at 600 mJ cm^{-2} and developed in AZ400K 1:3 for 6 min.

Thin copper electrical conduction layer would results in high electrical resistance and would generate significant amount of heat through Joule heating. In order to minimize Joule heating, we increased the thickness of the copper conduction layer to 1 μm. The substrate patterned with the stripline design was thermally evaporated (Auto 306, Edwards, UK) with 20 nm chromium as the seeding layer and 1 μm copper layer as the electrical conduction layer. Subsequently, lift-off process was performed on the evaporated substrate by washing the substrate in an acetone bath with ultrasonic agitation. During the lift-off process, the photoresist and excess copper layer was removed, leaving only the desired copper stripline on the substrate. The resistance of a square, R_S of 1 μm thick copper stripline is 16.8×10^{-3} ohm/sq. The resultant overall stripline resistance was about 3 ohm. Finally, silicon dioxide of 200 nm thick was grown using the Auto 306 e-beam evaporator. The contact pad is covered with glass slide during the evaporation to avoid silicone dioxide (SiO_2) from depositing onto the contact pads. The SiO_2 layer serves two purposes: (a) to insulate the current from short circuting when liquid is flowed into the microchannel; and (b) to facilitate bonding with PDMS microfluidic channel as PDMS generally does not adhere well directly onto copper surface.

The PDMS microchannel was fabricated using soft lithography technique. 25 μm thick SU8-3035 (MicroChem, USA) photoresist was spun at 2,500 rpm followed by softbake at 65°C for 2 min and 95°C for 7 min. The substrate was exposed at 180 mJ cm^{-2} and post exposure baked (PEB) at 65°C for 2 min and 95°C for 5 min. Subsequently, PDMS (Sylgard 184 10:1, Dow Corning, USA) was casted on the SU8 master and cured at 80°C for 6 h. The fabrication processes for the microchannel and micro stripline are summarized in Fig. 2. The overall dimension of the device is 35 mm × 35 mm. Finally, the microchannel is bonded onto the stripline with oxygen plasma treatment. We use SUSS MicroTec MJB4 mask aligner to

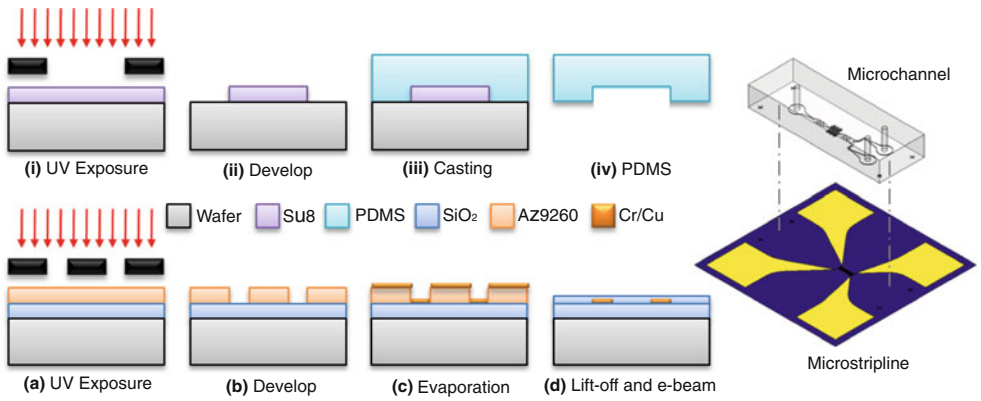

Fig. 2 **a** Overview of the device's fabrication process. Standard photolitography techniques are used to fabricate the microchannel and micro stripline. PDMS is casted on the SU8 master and heat cured at 80°C for 6 h. The square-meandering micro stripline of width 50 μm and aspect ratio of 3 is first patterned with AZ9260, followed by evaporation of Cr/Cu conduction layer and lift-off process. Subsequently, SiO_2 of 200 nm was grown onto the stripline for electrical insulation and to facilitate bonding with PDMS microchannel. **b** After exposing the chip and PDMS layer with oxygen plasma for surface activation, the microchannel was aligned and bonded to the chip with the help of four alignment marks. The dimension of the integrated chip is 35 mm × 35 mm

obtain a precise alignment between the microchannel and the stripline. The PDMS microchannel was placed onto a 5×5 inch^2 polymethyl methacrylate (PMMA) sheet and mounted on the MJB4 mask holder. The micro stripline is aligned to the microchannel by manually adjusting the *x*-, *y*-, and *z*-axis on the mask aligner. Once the alignment is done, the wafer is moved upward in the *z*-direction to bond with the PDMS. The bonded device is then left in oven for 4 h at 80°C to improve the adhesion between the wafer and PDMS.

2.3 Experimental setup

Current is supplied to the micro striplines via four probing pins (Coda Systems, UK). Once the probing pins are aligned to the device contact pads, the height of the adjustable post holder (07PCH514, CVI Melles Griot, US) is reduced such that the four pins are in firm contact with the contact pads. We fabricated an aluminium cooling pad with channels drilled within the cooling pad, allowing ice water (3–4°C) to flow in and out of the pad to remove the heat generated by the striplines.

Throughout all experiments, fluorescence magnetic microspheres COMPEL™ UMC4F/8741 COOH modified (Bangs Laboratories, USA) of 8.18 μm diameter are used. The excitation and emission wavelengths of the fluorescence beads are 480 and 520 nm, respectively. The magnetic beads are mixed with a buffer solution of 1:1 glycerol-DI water (density, $\rho = 1,126\,\mathrm{kg\,m^{-3}}$ and viscosity, $\eta = 9.01 \times 10^{-3}$ Pa s at 10°C), and are pumped into the microchannel with a syringe pump (LSP02-1B, China). The beads density is 1.554×10^6 beads/ml. The flow of magnetic particles in the sorting chamber is observed under SZX-16 (Olympus, Japan) stereomicroscope with KL2500 (Schott, Germany) fluorescence capable light source. The videos are captured with HDR-XR500E (Sony, Japan) with C-mount adaptor DCR TRV 950 (LM Scope, Austria).

In order to precisely control the switching frequency of the current supplied to the micro striplines, we built an electronic control box with a miniature electromagnetic relay (Fujitsu, Takamisawa RY-5WFZ-K). The maximum current rating for the relay is 2 A. Figure 3 shows the circuit diagram for the relay control. The relay is triggered on and off by using a TIP122 NPN transistor and a function generator (Agilent 33220A, USA). The left and right micro stripline are connected in normally closed and normally open configuration, respectively (i.e., current is always supplied to the left stripline and no current is supplied to right stripline when the relay is off). When the triggering signal from the signal generator is at on state, the transistor would be turned on, allowing the 5 V to be supplied to the relay. Once the relay is turned on, the current supply to the left stripline will be cut off while the right stripline circuit is connected and vice versa. Hence, we can switch the current supply to each stripline in turns (mutual exclusive configuration, [0–1, 1–0]) with accurate switching frequency.

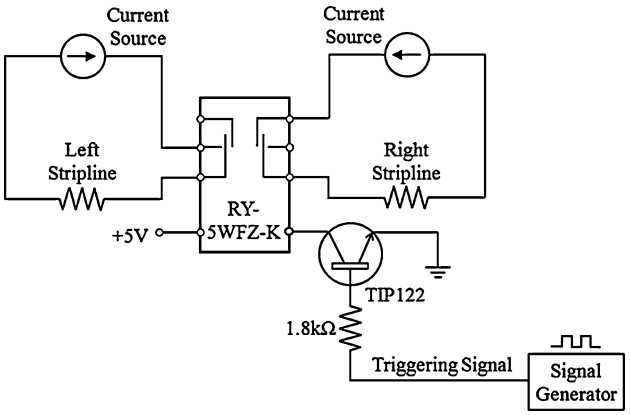

Fig. 3 Circuit diagram for controlling the current supplied to the left and right micro stripline. The relay is triggered on and off by an external function generator. The on-off state of the left and right stripline is mutually exclusive. If the left stripline is turned on, the right stripline would be turned off and vice versa

A Matlab (MathWorks, USA) program is written to quantify the sorting efficiency. The flow of fluorescence magnetic beads video is captured at 25 frames per second (fps) in high-definition (HD 1920 × 1080 MPEG4-AVC/H.264 format). The program first imports the frames of the video and converts the images into gray scale. The images are then further converted into binary images, *Im*, with the white pixels representing the magnetic beads. We remove the background noise by subtracting *Im* from the background image with no beads, *ImBG*. The image is split into top and bottom half and we quantify the normalized left-right sorting ratio (L/R ratio), α as follows:

$$\text{Left,} \quad L_t = \sum_{i=1}^{M/2} \sum_{j=1}^{S} (Im_{ij} - ImBG_{ij}), \tag{1}$$

$$\text{Right,} \quad R_t = \sum_{i=M/2+1}^{M} \sum_{j=1}^{S} (Im_{ij} - ImBG_{ij}), \tag{2}$$

$$\text{L/R Ratio,} \quad \alpha_t = \frac{L_t}{L_t + R_t}, \tag{3}$$

where $Im_{ij} \in [0,1]$, $ImBG_{ij} \in [0,1]$, $M =$ height of image, and $S =$ width of image in pixel. Im_{ij} and $ImBG_{ij}$ represent the pixel value at row i and column j for the captured image and background image, respectively. In order to systematically compare the sorting efficiency at different flow conditions, we compute the root mean square value (RMS) of the normalized sorting signal as follows:

$$\text{Sorting Efficiency RMS, } \epsilon = \alpha_{\text{avg}} + \sqrt{\frac{\sum_{t=1}^{N}(\alpha_t - \alpha_{\text{avg}})^2}{N}}, \tag{4}$$

where $\alpha_{\text{avg}} = \frac{1}{N}\sum_{t=1}^{N}\alpha_t$ and N is the total number of frames.

3 Results and discussions

In the presence of magnetic fields, magnetic beads are forced to change its flow path and choose a streamline closer to the field generating stripline. Figure 4 shows the fluorescence image of the magnetic beads flow at different conditions: (a) splitting (no current), (b) left sorting with a current of 2 A, and (c) right sorting with a current of 2 A at a total flow rate of 200 μl h^{-1}. In Fig. 4b, c, we observed that the magnetic beads velocity is significantly reduced when the stripline current is turned on. The beads are attracted and pulled towards the stripline surface by the magnetic forces generated. The additional frictional force between the stripline surface and the bead causes the bead to slow down to a velocity of approximately 0.511 mm s^{-1}. Once the bead escapes the sorting chamber, the bead velocity increases to approximately 2.78 mm s^{-1}. The velocity of the bead was estimated by dividing the length of the bead's streak line with the reciprocal of the number of frame per second image capturing speed.

The sorting efficiency of our system is as high as 95% for a sorting period of more than or equal to 2 s. Figure 5 shows the L/R ratio variation for sorting periods of 0.5, 1, 2, 5, and 10 s at a total flow rate of 2,000 μl h^{-1} and a stripline current of 2 A. At a switching frequency of 2 Hz, the L/R ratio variation is sinusoidal rather than a square wave. This suggests that the switching frequency has approached the system response (or delay) time. As the switching period increases, we observe better defined square wave form for the L/R ratio. The rise time is approximately 0.25 s, corresponding to the fastest switching period of 0.5 s.

There are two important factors in determining the success rate of the bead sorting: (a) applied current and (b) flow rate. These two factors are affecting the sorting efficiency in a contrasting manner. From Biot–Savart law, we know that the magnetic flux density, B at distance R from the stripline is given by (Ramadan et al. 2004):

$$B = \frac{\mu_0 I}{4\pi}\int \frac{\mathrm{d}l \times \hat{r}}{|r|^2}, \tag{5}$$

which suggests that the magnetic flux density, B is proportional to the applied current, I (Eq. 5). The magnetic energy component can be expressed as:

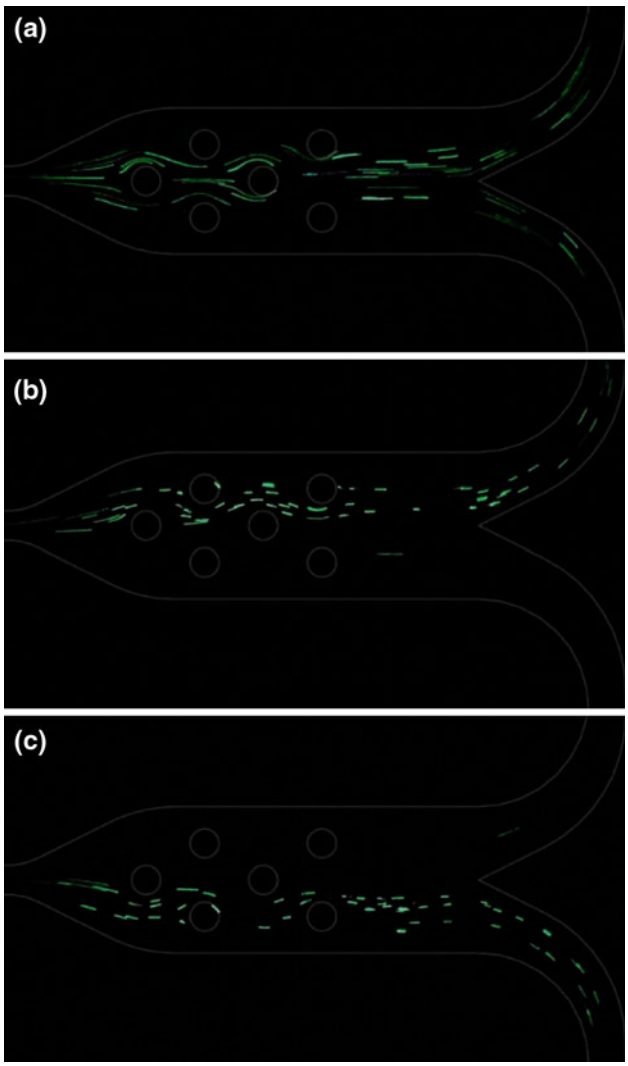

Fig. 4 Fluorescent image of the magnetic beads flow at different conditions $Q_{\text{total}} = 200$ μl h^{-1}: **a** splitting (no applied current), **b** left sorting (left stripline current = 2 A) and **c** right sorting (right stripline current = 2 A). The *gray lines* are added to represent the outlines of the channel wall. The magnetic beads are focused in the core stream by means of hydrodynamic focusing. The beads enter the sorting chamber at the center and split equally to the two outlets. When current is applied to one of the striplines, the beads are forced to change its flow direction and switch to another streamline closer to the field generating micro stripline. Thus, the magnetic beads can be manipulated and forced to exit at a desired outlet by gradually changing the flow path of the beads

$$E_{\text{magnetic}} = \frac{B^2}{2\mu}(\propto I^2 \because B \propto I), \tag{6}$$

where μ is the magnetic permeability of the magnetic bead. Since the bead switches its outlet when there exist a magnetic force component in the y-axis, we can infer the sorting efficiency from the beads' magnetic energy:

$$\epsilon \propto E_{\text{magnetic}} \propto I^2. \tag{7}$$

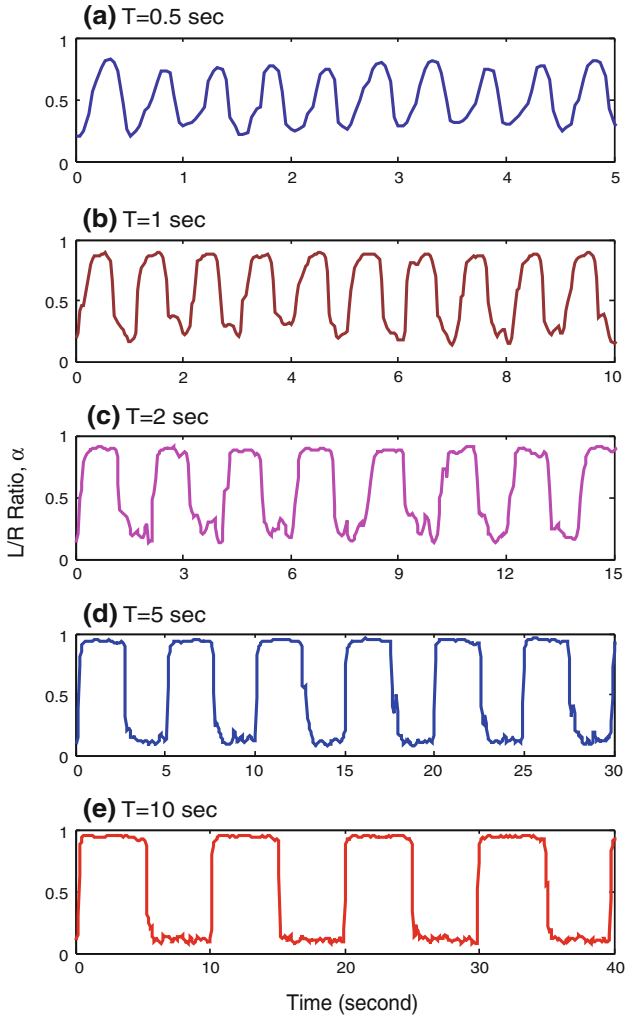

Fig. 5 The L/R ratio for sorting periods of **a** 0.5, **b** 1, **c** 2, **d** 5, and **e** 10 s for a total flow rate of 2,000 μl h^{-1} and stripline current of 2 A. The L/R ratio increases with sorting period. The fastest achievable switching frequency is 2 Hz (or 0.5 s periods). The sorting efficiency is as high as 95% (L/R ratio of 0.9) for sorting period ≥ 2 s

Therefore, the sorting efficiency is proportional to the square of the current applied to the stripline.

Figure 6a shows that the sorting efficiency increases with the applied current. In order to verify the quadratic relationship between the sorting efficiency and applied current experimentally, we numerically determine the coefficients of the following polynomial equation:

$$\epsilon = kI^n + c, \tag{8}$$

$$\log(\epsilon - c) = \log k + n \log I. \tag{9}$$

The intercept coefficient, c represents the sorting efficiency RMS when the applied current is zero, and should be 0.5 under ideal condition. However, the coefficient c was determined to be 0.537 experimentally. The slight deviation is due to the difference in the fluidic resistance between the left and right outlets, and the random entrance position of magnetic beads at the inlet of the sorting chamber. The coefficient n and k were estimated from the gradient and the interception of the graph $\log(\varepsilon - c)$ vs. $\log(I)$, respectively, and are summarized in Table 1.

Table 1 Summary of the statistical values for the n, k, r^2 coefficients for the experimental data shown in Fig. 6a

Q (μl h^{-1})	n	k ($\times 10^{-2}$)	r^2
1,000	1.92	7.92	0.9998
2,000	2.12	6.14	0.9987
3,000	2.23	5.20	1.0000

The average experimental value for n is 2.09 ± 0.16, while the square of the correlation coefficient, r^2 for the linear fitting is almost 1. Hence, our hypothesis for the square relationship between the sorting efficiency and applied current is verified experimentally. Furthermore, the experimental results are also consistent with our simulation results for the variation of the y-component magnetic bead force, F_y with the applied current (refer to Appendix 1). The higher the applied current, the stronger will be the magnetic forces on the magnetic beads.

On the other hand, the sorting efficiency decreases with increasing buffer flow rate (refer to Fig. 6b). Since the magnetic beads are hydrodynamically focused in the core stream while entering the sorting chamber, the beads spread a width of w (while the sorting chamber has a width of W). A magnetic bead switches its outlet if $t_{w/2} \leq t_L$, where $t_{w/2}$ represents the time needed for a magnetic bead to travel vertically (in the y-direction) from core-side stream interface to the middle axis of the sorting chamber and t_L is the time needed for a bead to travel through the the sorting chamber of length L. Assuming the average flow velocity, v is given by the ratio of the buffer flow rate, Q to the sorting chamber's cross sectional area, A ($v = Q/A$), we arrived at the following phenomenological relationship for the sorting condition:

$$t_L \approx \frac{L}{v} = \frac{LA}{Q}, \tag{10}$$

$$t_{w/2} \leq \frac{LA}{Q}. \tag{11}$$

Increasing the buffer flow rate, Q would decrease the fraction LA/Q and t_L. For the sorting condition in Eq. 11 to hold true at higher flow rate, the system has shorter time, $t_{w/2}$, to attract the beads towards the desired outlet. Hence, increasing the buffer flow rate would lower the sorting efficiency.

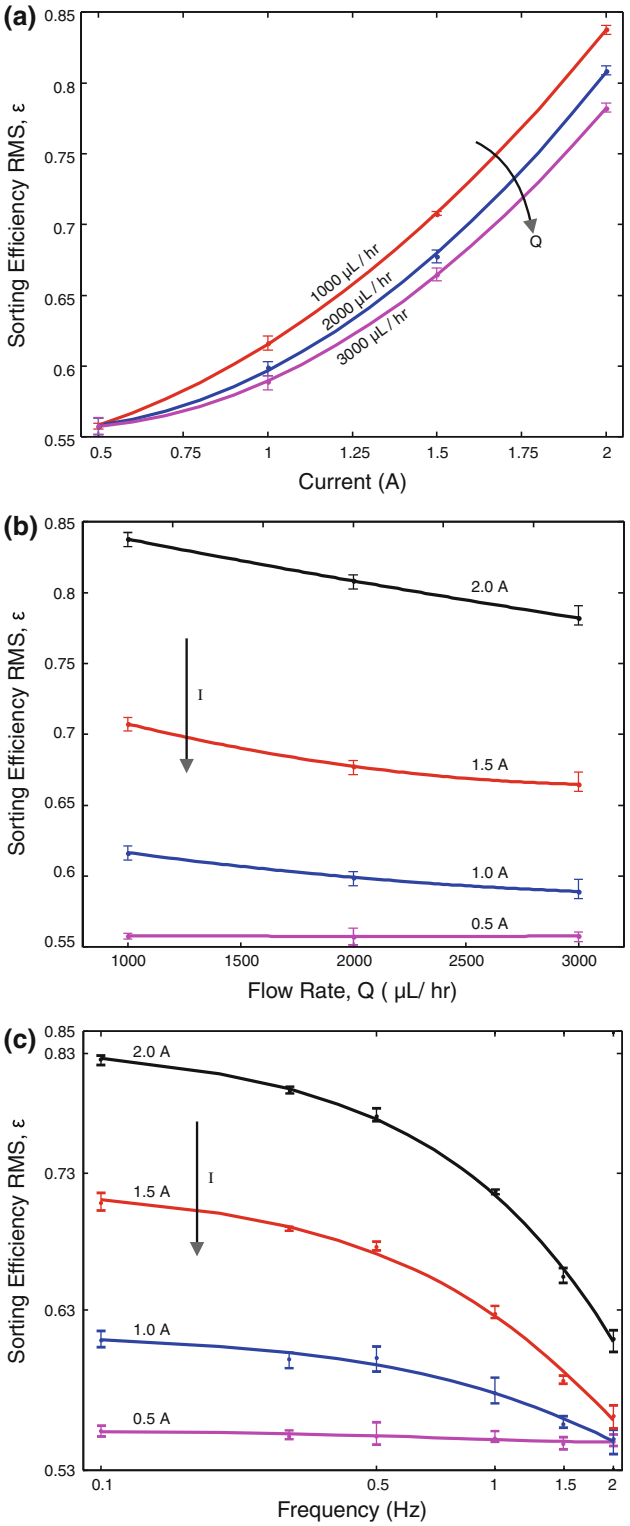

◀ **Fig. 6** Experimental results: the effect of **a** applied current, **b** buffer flow rate, and **c** switching frequency on the sorting efficiency (RMS). The switching frequency is fixed at 0.05 Hz for experiments (**a**) and (**b**), while the total flow rate is fixed at 1,000 µl h^{-1} for experiment (**c**). The sorting efficiency is proportional to the square of current applied to the stripline. The stronger magnetic forces generated at higher applied current results in higher success rate of sorting the beads to the desired outlet. On the other hand, at the same applied current, the sorting efficiency decreases with increasing buffer flow rate. The system behaves like a low pass RC circuit where the sorting efficiency decreases with switching frequency

In addition, the sorting efficiency is also affected by the switching frequency. Figure 6c shows that the sorting efficiency decreases with increasing switching frequency for flow at 1,000 µl h^{-1}. As the switching period approaches the time required to alter the flow path of the beads, the sorting efficiency would decrease. The force balance equation for the magnetic bead in the y-direction is $m\ddot{y} + \beta\dot{y} = F_{\text{magnetic}}$, where m is the mass of the bead, $\beta = 3\pi\eta D_{\text{p}}$, η is the medium viscosity, and D_{p} is the bead's diameter. In analogy to a low pass RC filter circuit, the cut off frequency $\left(f_{\text{c}} = \frac{1}{2\pi\text{RC}}\right)$ for our system is:

$$f_{\text{c}} = \frac{\beta}{2\pi m} = \frac{3\pi\eta D}{2\pi m} \approx 360\,\text{kHz}, \tag{12}$$

where $m = 3.07 \times 10^{-13}$ kg, $\eta = 9.01 \times 10^{-3}$ Pa s, and $D = 8.18$ µm. The cut off frequency is significantly higher than the achievable sorting frequency of 2 Hz. In other words, the inertia effect is negligible.

In fact, there exists a physical limitation to the sorting frequency that could be achieved by the device. From Eq. 11, we could deduce that the cut off frequency is greater or equal to the reciprocal of the particle travel time, t_{L}. Assuming that the total flow rate, Q is 1,000 µl h^{-1} and the cross sectional area of the channel, A is 25 µm × 1,000 µm the time, t_{L} required for a bead to travel through the sorting chamber of length 3,500 µm is approximately 0.315 s (or 3.17 Hz). Hence, the limiting switching frequency is in the order of several hertz. This agrees well the fastest achievable experimental switching speed of 2 Hz. In order to achieve a faster switching response, we need to increase the buffer flow rate and magnitude of the magnetic forces on the magnetic beads, and also reduce the delay caused by the electronics switching box.

4 Conclusion

In conclusion, we have successfully designed, fabricated and implemented an integrated on-chip microfluidic device to demonstrate magnetic particle separation. Our device can effectively switch magnetic particles to the desired outlet with efficiency of up to 95% and achieved a fastest sorting frequency of 2 Hz. The limiting switching (or cut-off) frequency is found to be dependent on beads velocity, and the length and cross sectional area of the sorting chamber. We have investigated the effect of applied current, flow rate, and switching frequency on the sorting

efficiency. From the experimental results and theoretical analysis, we can conclude the following: (a) the sorting efficiency is proportional to the square of current applied to the stripline; (b) the sorting efficiency decreases with increasing buffer flow rate; and (c) the sorting efficiency decreases with higher switching frequency. With the ability to cleanly switch magnetic beads to the desired outlets, our system has huge potential to be integrated as part of a biomedical lab-on-chip device.

Acknowledgments This study was supported by the Singapore's Agency for Science, Technology and Research (A*STAR SERC grant: 082 101 0015) and the Singapore-French MERLION programmes. The authors would also like to acknowledge Mr. Chun Fan Goh for the helpful discussion on image processing and electronic circuit.

Appendix 1: Magnetic forces generated by square meandering micro stripline

In order to have a better understanding of the magnetic field strength and the magnetic forces acting on magnetic beads, we utilized the 3-D magnetostatics toolbox in COMSOL multiphysics (COMSOL Inc, USA) to simulate the magnetic field distribution of the micro stripline. Figure 7 shows the COMSOL multiphysics simulation results for the magnetic flux density (a) B_x, (b) B_y, and (c) B_z with an applied current of 2 A and at a height of 10 μm from the copper stripline surface. The stripline has a width of 50 μm and the height-width ratio is 3. The current is set to flow in the left to right configuration. The highest magnetic flux density for the x-, y-, and z-component is approximately 18 mT. In the simulation, we made the following assumptions: the magnetic field is only generated by the current applied to the stripline, the magnetic field is measured in free-space, the current flow is steady, and the magnetic field is not permeating the air box surface. The boundary conditions of the encapsulating box were set to magnetic insulation and electric insulation while the boundary condition of the stripline was set to continuity.

Magnetic beads are attracted to the magnetic field generated by the current-carrying micro stripline. The magnetic force acting on a magnetic bead is governed by (Pamme 2005; Shevkoplyas et al. 2007; Beyzavi and Nguyen 2008):

$$F = \frac{V\Delta\chi}{\mu_0}(\mathbf{B}\cdot\nabla)\mathbf{B} = F_x\mathbf{i} + F_y\mathbf{j} + F_z\mathbf{k}, \tag{13}$$

where

$$F_x = \frac{V\Delta\chi}{\mu_0}\left(B_x\frac{\partial B_x}{\partial x} + B_y\frac{\partial B_x}{\partial y} + B_z\frac{\partial B_x}{\partial z}\right), \tag{14}$$

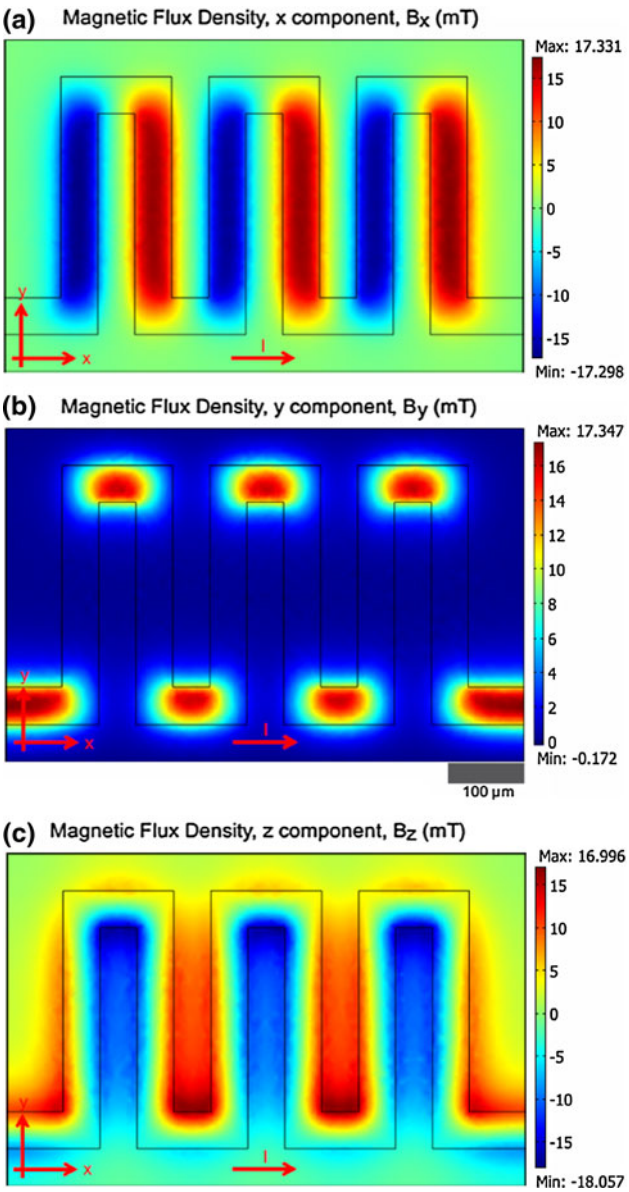

Fig. 7 Contour plot of the **a** x-, **b** y-, and **c** z-component magnetic flux density at an applied current of 2 A and at a vertical distance of 10 μm from the stripline. The width of the square meandering micro stripline is 50 μm and its height–width ratio is 3. The maximum magnetic flux density generated with 2 A current is approximately 18 mT

$$F_y = \frac{V\Delta\chi}{\mu_0}\left(B_x\frac{\partial B_y}{\partial x} + B_y\frac{\partial B_y}{\partial y} + B_z\frac{\partial B_y}{\partial z}\right), \tag{15}$$

$$F_z = \frac{V\Delta\chi}{\mu_0}\left(B_x\frac{\partial B_z}{\partial x} + B_y\frac{\partial B_z}{\partial y} + B_z\frac{\partial B_z}{\partial z}\right), \tag{16}$$

V is the volume of the magnetic bead, $\Delta\chi$ is the difference in magnetic susceptibilities between the magnetic particle and its surrounding buffer, B is the magnetic flux density,

and μ_0 is the magnetic constant $4\pi \times 10^{-7}\,\mathrm{T\,mA^{-1}}$. After obtaining the magnetic flux density from COMSOL, we can compute the force acting on a magnetic bead using Eq. 14–16. The partial derivative of B_x, B_y, and B_z in the x-, y- and z-direction can be computed using the matrix operation as follows:

$$\frac{\partial A}{\partial x} = MA^T,\ \frac{\partial A}{\partial y} = MA,\ \frac{\partial A}{\partial z} = A_{k+1} - A_k, \tag{17}$$

where A represents B_x, B_y, and B_z, k is the index representing the kth simulation plane in the z-axis and

$$M = \begin{pmatrix} -1 & 1 & & & \\ & -1 & 1 & & \\ & & \ddots & \ddots & \\ & & & -1 & 1. \end{pmatrix} \tag{18}$$

Figure 8 shows the simulation results for the variation of the maximum y-component of $(\mathbf{B}\cdot\nabla)\mathbf{B}$, which is proportional to the magnetic bead force in the y-direction, F_y, with the applied current at a vertical distance of 5, 10, and 15 μm from the stripline surface. From the figure, we can deduce that the maximum y-component magnetic force is proportional to the square of the applied stripline current. The magnetic bead forces decreases with height from the stripline surface. The simulation results for the maximum magnetic forces of x- and z-components also show similar variation trend with the applied current (not shown).

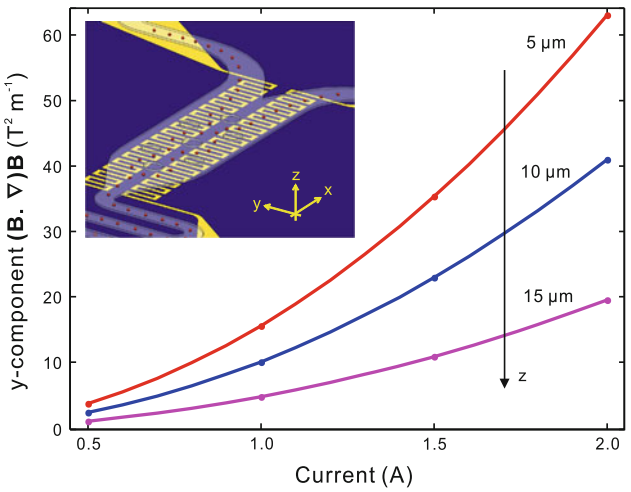

Fig. 8 Simulation results for the effect of applied current on the maximum y-component of $(\mathbf{B}\cdot\nabla)\mathbf{B}$, which is proportional to the magnetic bead force in the y-direction, F_y, at a vertical distance of 5, 10, and 15 μm from the stripline surface. The maximum y-component magnetic force increases with the square of the applied stripline current. Further from the stripline surface, the magnetic forces on the magnetic beads are weaker. The inset is a schematic illustration of the striplines configuration in the microfluidic sorting chamber

Appendix 2: Gravitational settling and wall effect

The magnetic beads tend to sink to the bottom of the channel surface due to the density difference and gravity effect (Li and Daghighi 2010). The sediment velocity of a particle is given by (Huh et al. 2007):

$$U_{\mathrm{sed}} = \frac{2r^2 g\Delta\rho}{9\mu}, \tag{19}$$

where r is the radius of particles, g is gravitational acceleration, $\Delta\rho$ is the density difference between particle and carrier liquid, and μ is the viscosity of buffer. With the diameter of 8 μm and density of the magnetic beads is $1.07\,\mathrm{g\,cm^{-3}}$, and carrier liquid density of $1.126\,\mathrm{g\,cm^{-3}}$ and viscosity of 9.01×10^{-3} Pa s, the sedimentation velocity is $2.17 \times 10^{-7}\mathrm{ms^{-1}}$. Without the presence of the magnetic force, the time taken for a bead to sink to the bottom surface for a 25 μm high channel is about 115 s. Since the lowest flow rate used in the experiment is 200 $\mu\mathrm{l\,h^{-1}}$, the slowest average time taken for a particle to travel past the sorting chamber of length 3,500 μm approximately 1.6 s. Hence, the gravitational settling effect is negligible.

In addition, due to the low channel height to bead diameter ratio, there bound to be increased hydrodynamic drag force caused by the wall effect in the vertical direction. However, the wall effect is insignificant in the lateral direction ($x - y$ plane) since the width and length of the sorting chamber are 1,000 and 3,500 μm, respectively, while the bead diameter is only 8 μm. The success rate of sorting the beads to the desired outlet depends on the ability of the device to attract the beads in the y-direction. Therefore, the wall effect on the hydrodynamic force is not considered in this study.

References

Bange A, Halsall HB, Heineman WR (2005) Microfluidic immunosensor systems. Biosens Bioelectron 20:2488–2503

Bashir R (2004) Biomems: state-of-the-art in detection, opportunities and prospects. Adv Drug Delivery Rev 56:1565–1586

Beyzavi A, Nguyen NT (2008) Modeling and optimization of planar microcoils. J Micromech Microeng 18:095,018

Choi JW, Liakopoulos TM, Ahn CH (2001) An on-chip magnetic bead separator using spiral electromagnets with semi-encapsulated permalloy. Biosens Bioelectron 16:409–416

Choi JW, Oh KW, Thomas JH, Heineman WR, Halshall HB, Nevin JH, Helmicki AJ, Henderson HT, Ahn CH (2002) An integrated microfluidic biochemical detection system for protein analysis with magnetic bead-based sampling capabilities. Lab Chip 2:27–30

Deng T, Prentiss M, Whitesides GM (2002) Fabrication of magnetic microfiltration systems using soft lithography. Appl Phys Lett 80:461–463

Gijs MAM (2004) Magnetic bead handling on-chip: new opportunities for analytical applications. Microfluid Nanofluid 1:22–40

Gijs MAM, Lacharme F, Lehmann U (2010) Microfluidic applications of magnetic particles for biological analysis and catalysis. Chem Rev 110:1518–1563

Huh D, Bahng JH, Ling Y, Wei HH, Kripfgans OD, Fowlkes JB, Grotberg JB, Takayama S (2007) Gravity-driven microfluidic particle sorting device with hydrodynamic separation amplification. Anal Chem 79:1369–1376

Inglis DW, Riehn R, Austin R, Strum J (2004) Continuous microfluidic immunomagnetic cell separation. Appl Phys Lett 85:5093–5095

Jiang Z, Llandro J, Mitrelias T, Bland JAC (2006) An integrated microfluidic cell for detection, manipulation, and sorting of single micron-sized magnetic beads. J Appl Phys 99:08S105

Kim DH, Rozhkova EA, Ulasov IV, Bader SD, Rajh T, Lesniak MS, Novosad V (2010) Biofunctionalized magnetic-vortex microdiscs for targeted cancer-cell destruction. Nat Mater 9:165–171

Kose AR, Fischer B, Mao L, Koser H (2009) Label-free cellular manipulation and sorting via biocompatible ferrofluids. Proc Natl Acad Sci USA 106:21,478–21,483

Lee C, Lee H, Westervelt RM (2001) Microelectromagnets for the control of magnetic nanoparticles. Appl Phys Lett 79:3308–3310

Lee H, Purdon AM, Chu V, Westervelt RM (2004) Controlled assembly of magnetic nanoparticles from magnetotactic bacteria using microelectromagnets array. Nano Lett 4:995–998

Lee H, Liu Y, Ham D, Westervelt RM (2007) Integrated cell manipulation systemcmos/microfluidic hybrid. Lab Chip 7: 331–337

Lee WC, Lien KY, Lee GB, Lei HY (2008) An integrated microfluidic system using magnetic beads for virus detection. Diagn Microbiol Infect Dis 60:51–58

Li D, Daghighi Y (2010) Eccentric electrophoretic motion of a rectangular particle in a rectangular microchannel. J Colloid Interface Sci 342:638–642

Lim C, Zhang Y (2007) Bead-based microfluidic immunoassays: the next generation. Biosens Bioelectron 22:1197–1204

Liu C, Lagae L, Wirix-Speetjens R, Borghs G (2007a) On-chip separation of magnetic particles with different magnetophoretic mobilities. J Appl Phys 101:024,913

Liu YJ, Guo SS, Zhang ZL, Huang WH, Baigl D, Xie M, Pang YCDW (2007b) A micropillar-integrated smart microfluidic device for specific capture and sorting of cells. Electrophoresis 28:4713–4722

Nguyen NT, Ng KM, Huang X (2006) Manipulation of ferrofluid droplets using planar coils. Appl Phys Lett 89:052,509

Pamme N (2005) Magnetism and microfluidics. Lab Chip 6:24–38

Pamme N, Wilhelm C (2006) Continuous sorting of magnetic cells via on-chip free-flow magnetophoresis. Lab Chip 6:974C980

Ramadan Q, Samper V, Poenar D, Yu C (2004) On-chip microelectromagnets for magnetic-based bio-molecules separation. J Magn Magn Mater 281:150C172

Ramadan Q, Samper V, Poenar DP, Yu C (2006) An integrated microfluidic platform for magnetic microbeads separation and confinement. Biosens Bioelectron 21:1693–1702

Rida A, Fernandez V, Gijs MAM (2003) Long-range transport of magnetic microbeads using simple planar coils placed in a uniform magnetostatic field. Appl Phys Lett 83:2396–2398

Rong R, Choi JW, Ahn CH (2006) An on-chip magnetic bead separator for biocell sorting. J Micromech Microeng 16: 2783–2790

Shevkoplyas SS, Siegel AC, Westervelt RM, Prentiss MG, Whitesides GM (2007) The force acting on a superparamagnetic bead due to an applied magnetic field. Lab Chip 7:1294–1302

Shikida M, Koyama M, Nagao N, Imai R, Honda H, Okochi M, Tsuchiya H, Sato K (2009) Agitation of magnetic beads by multi-layered flat coils. Sens Actuators B 137:774–780

Smistrup K, Tang PT, Hansen O, Hansen MF (2006) Microelectromagnet for magnetic manipulation in lab-on-chip systems. J Magn Magn Mater 300:418–426

Song SH, Lee HL, Min YH, Jung HI (2009) Electromagnetic microfluidic cell labeling device using on-chip microelectromagnet and multi-layered channels. Sens Actuators B 141: 210–216

Speetjens RW, de Boeck J (2004) On-chip magnetic particle transport by alternating magnetic field gradients. IEEE Trans Magn 40:1944–1946

Wang ZH, Lew WS, Bland JAC (2006) Manipulation of superparamagnetic beads using on-chip current lines placed on a ferrite magnet. J Appl Phys 99:08P104